Atmos. Chem. Phys. Discuss., doi:10.5194/acp-2017-116, 2017
Manuscript under review for journal Atmos. Chem. Phys.
Discussion started: 15 March 2017

Atmospheric Chemistry and Physics Discussions

The role of traffic emissions in particulate organics and nitrate at a downwind site in the periphery of Guangzhou, China

Yi Ming Qin[1], Hao Bo Tan[2], Yong Jie Li[3,*], Misha I. Schurman[4], Fei Li[2], Francesco Canonaco[5], André S. H. Prévôt[5], Chak K. Chan[1,4,6,*]

[1]Department of Chemical and Biomolecular Engineering, Hong Kong University of Science and Technology, Hong Kong, China

[2]Institute of Tropical and Marine Meteorology, China Meteorological Administration, Guangzhou, China

[3]Department of Civil and Environmental Engineering, Faculty of Science and Technology, University of Macau, Taipa, Macau, China

[4]Division of Environment, Hong Kong University of Science and Technology, Hong Kong, China

[5] Laboratory of Atmospheric Chemistry, Paul Scherrer Institute, 5232, Villigen PSI, Switzerland

[6]School of Energy and Environment, City University of Hong Kong, Hong Kong, China

[*]To Whom Correspondence Should be Addressed

Chak K. Chan: AC1-G5716, School of Energy and Environment, City University of Hong Kong, Tat Chee Avenue, Kowloon, Hong Kong, China
Tel: (852) 3442-5593; Fax: (852) 3442-0688
Email: chak.k.chan@cityu.edu.hk

Yong Jie Li: E11-3017, Faculty of Science and Technology, University of Macau, E11, Avenida da Universidade, Taipa, Macau, China
Tel: (853) 8822-4943; Fax: (853) 8822-2426
Email: yongjieli@umac.mo

Atmos. Chem. Phys. Discuss., doi:10.5194/acp-2017-116, 2017
Manuscript under review for journal Atmos. Chem. Phys.
Discussion started: 15 March 2017

Abstract:

Particulate matter (PM) pollution on the peripheries of rapidly expanding megacities in China can be as serious as in the cities due to direct emission and transport of primary PM from cities and effective formation of secondary PM. To investigate the emission and formation of PM on the periphery of Guangzhou (a megacity in southern China), a suite of real-time instruments were deployed at Panyu, downwind of Guangzhou, for PM measurements from November to December 2014. Dominated by organics, PM_1 (particles with diameter less than 1 μm) concentrations in Panyu were higher (average ~55.4 μg/m^3) than those in nearby cities such as Hong Kong and Shenzhen. Five sources for organic aerosols (OA) were resolved by positive matrix factorization (PMF) analysis with the multilinear engine (ME-2). These sources are hydrocarbon-like organic aerosol (HOA), cooking organic aerosol (COA), biomass burning related organic aerosol (BBOA), as well as semi-volatile oxygenated organic aerosol (SVOOA) and low-volatile oxygenated organic aerosol (LVOOA). The use of the COA mass spectrum obtained in our earlier study at a urban site in Hong Kong as a constraining factor in ME-2 produced the most interpretable results for the Panyu dataset. Freshly emitted HOA contributed 40% to the high concentrations of organics at night. The mass concentration of SOA (SVOOA+LVOOA) continuously increased as odd oxygen ($O_x = O_3 + NO_2$) increased during daytime, attributable to the secondary production of PM facilitated by photochemistry. The SOA-to-O_x ratio was higher than those reported in previous studies in North America (covering the period from spring to summer), indicating efficient photochemical production of SOA even in late autumn and early winter at this subtropical downwind site. The efficient SOA formation during daytime was likely fueled by the sufficient SOA precursors in the atmosphere. The large input of NO_x, which tracked well with HOA from automobile emissions, resulted in the significant formation of nitrate in both daytime and nighttime. Strong correlations between particulate nitrate and excess ammonium ($[NH_4^+]/[SO_4^{2-}] - 1.5) \times [SO_4^{2-}]$) were observed. Higher partitioning of nitrate into the gas phase was found in November than in December, likely due to the lower temperatures in December. Results from this study suggest that there is much room to mitigate the PM pollution in urbanized areas such as Guangzhou, as well as their peripheries, by reductions in traffic-related pollutants.

Atmos. Chem. Phys. Discuss., doi:10.5194/acp-2017-116, 2017
Manuscript under review for journal Atmos. Chem. Phys.
Discussion started: 15 March 2017

1. Introduction:

The Pearl River Delta (PRD) economic zone is one of the most urbanized and industrialized regions in China, producing about 19% of China's gross domestic product each year (Zhong et al., 2013). The fast economic development in the PRD has led to rapid deterioration in air quality (Chan and Yao, 2008; Ho et al., 2003). The PRD is situated in a subtropical region where photochemistry may differ from those in other urbanized city clusters in China. For instance, the relatively high photochemical activity, high temperature, and high relative humidity (RH) in this subtropical region facilitate effective secondary formation of particulate matter (PM) in PRD (Lee et al., 2013; Li et al., 2013; Qin et al., 2016a). With densely populated cities including two megacities Guangzhou and Shenzhen and other smaller but also highly urbanized ones, the PRD region is emerging into a giant city cluster. There are, nevertheless, some less populated areas between those cities and presumably can serve as a "buffer" zone in regional air quality. Given the complex and non-linear processes in secondary production of PM, the impacts of the adjacent cities to the air quality of these "buffer" areas can be crucial but they have not been thoroughly investigated.

Over the last decade, many studies in PRD have revealed that organic aerosols (OA) and sulfate are the most abundant components of fine particles (e.g., Hagler et al., 2006; Huang et al., 2006; Louie et al., 2005). The main precursor of sulfate, SO_2, began to decrease since 2006, because of the widespread application of flue-gas desulfurization devices in power plants in response to a new policy implemented by the Chinese government (Lu et al., 2010; Zhang et al., 2012b). Over the same period, however, emissions from vehicles, e.g. NO_x, volatile organic compounds (VOCs), black carbon (BC) and traffic-related organics, however, have increased (Wang et al., 2013; Zhang et al., 2012a). A recent study showed that 4.16 million tons (Mt) of hydrocarbon, 7.72 Mt of NO_x, and 0.37 Mt of $PM_{2.5}$ (particles with diameter less than 2.5 micron) were produced by vehicular emissions in China in 2013 (Wu et al., 2016). Although the high-polluting vehicles (such as heavy-duty diesel trucks) are not allowed to enter the inner areas of many megacities during the day in China, they are nevertheless active at night until early morning, especially on the peripheries of these cities. This regulatory policy results in nighttime peaks in vehicular pollutants commonly observed in many cities in China (Zhang and Cao, 2015). The oxidation of traffic-related gaseous pollutants (e.g., NO_x and VOCs) leads to generally less volatile products, which have the tendency to either nucleate or condense onto pre-existing particles (Hallquist et al., 2009), result in the

formation of secondary PM. Particles from vehicle exhaust, such as hydrocarbon-like organic aerosol (HOA), can also undergo chemical transformation in the atmosphere (Zhang et al., 2015) and lead to photochemical smog on the following day.

To better understand the impact of traffic emissions in Guangzhou to its peripheral areas, we deployed an Aerodyne HR-ToF-AMS at a site downwind Guangzhou in late autumn to early winter 2014, during a period of prevailing northerly winds, to measure non-refractory PM_1 (NR-PM_1). Factor analysis of OA for source apportionment was performed with a new positive matrix factorization (PMF) procedure using the multilinear engine (ME-2) with the source finder (SoFi) (Canonaco et al., 2013). The procedure allows an effective exploration of the solution space, a more objective selection of the best solution, and an estimation of the rotational uncertainties (Canonaco et al., 2013; Crippa et al., 2014; Elser et al., 2016; Fröhlich et al., 2015; Paatero and Hopke, 2009). The source and formation of nitrate and SOA at this downwind site of Guangzhou will be discussed in detail.

2. Method

2.1. Sampling site description

The sampling site is located at Panyu District, a downwind site from downtown Guangzhou. This suburban site is about 15 km south of the city center (Tan et al., 2013; Zou et al., 2015; Cheung et al., 2016). It is located at the summit of Dazhengang (23°00 N, 113°21 E) at an altitude of about 150 m (Fig. S1 in the Supplement) and surrounded by residential neighborhoods with no significant industrial sources nearby. Ambient sampling was conducted from November 07th, 2014 to January 3rd, 2015.

2.2. Measurements

In the HR-ToF-AMS measurements (DeCarlo et al., 2006), ambient air was sampled through a $PM_{2.5}$ cyclone on the rooftop, with a flow rate of approximately 0.084 L/min drawn by the AMS and the remainder drawn by an auxiliary pump. A diffusion drier was used to dry the sampled air stream, which reduced the RH of air to below 30 % before going into the HR-ToF-AMS. Other data presented in this work were obtained from collocated instruments, which included a Grimm 180 for $PM_{2.5}$, a thermo-optical ECOC analyzer (Sunset Laboratory Inc.), a Magee AE33, a dual spot filter based instrument for black carbon (Drinovec et al., 2015), a gas analyzer system (Teledyne Instruments), and a monitor for aerosols and gases in ambient air (MARGA). The $PM_{2.5}$

mass concentration by Grimm 180 was corrected by the daily $PM_{2.5}$ mass concentration with quartz filter measurement. Meteorological data (e.g. wind, temperature and RH) were obtained from a weather station located near the sampling site. Solar irradiance data were measured from a station in Nansha District, around 27.5 km from the sampling site. Particle liquid water content (LWC) was estimated by Aerosol Inorganic Model (E-AIM II) (Clegg et al., 1998). The AMS collected 5-minute average particle mass spectra spanning from m/z 12 to 300 for the V + particle time-of-flight (pToF) mode (high sensitivity) and the W mode (high resolution). And the dataset were only analyzed with m/z below 200 for the high resolution analysis. AMS calibrations, including ionization efficiency (IE) calibration, flow rate calibration, and size calibration, as well as data quality assurance protocols were used (DeCarlo et al., 2006; Lee et al., 2013; Schurman et al., 2015). IE calibrations with DMA size-selected (mobility diameter, D_m= 400 nm) pure ammonium nitrate particles were carried out weekly. Filtered ambient air with a HEPA filter was sampled on a daily basis for 30 minutes to obtain background signals. Flow rate calibrations with a Gilian Gilibrator and PToF size calibrations were made with Nanosphere TM PSL particles (Duke Scientific, Palo Alto, CA, USA) and ammonium nitrate particles with selected size by scanning mobility particle sizer (SMPS) in the range of 178 to 800 nm were performed both before and after the sampling campaign. Gaseous CO_2 contributions to m/z 44 were quantified using a CO_2 monitor (PICARRO 2301).

2.3. Data analysis

AMS data analysis was performed using the SQUIRREL (v1.56D) and PIKA (v1.15D) toolkits written in Igor Pro 6.37A (WaveMetrics Inc., Lake Oswego, OR) (http://cires1.colorado.edu/jimenez-group/ToFAMSResources/ToFSoftware/index.html). Default relative ionization efficiency (RIE) values of 1.2 for sulfate, 1.1 for nitrate, 1.3 for chloride, and 1.4 for organics were used. The ammonium RIE of 4.7 was chosen as the average from IE calibrations. To account for particle losses within the instrument, a particle collection efficiency factor (CE) was used. The influence of RH in this study is considered minor, as a diffusion drier kept the sampling line RH consistently below 30%. Under these conditions, the Middlebrook parameterization would suggest a CE of ~45–50% based on the measured inorganic constituents. However, organic compounds, less bouncy than inorganics, dominated at the measurement site. They may also hinder the complete efflorescence of particles in the drier and further reduce the particle bounce effect and increase the particle collection efficiency. The mass concentrations of

Atmos. Chem. Phys. Discuss., doi:10.5194/acp-2017-116, 2017
Manuscript under review for journal Atmos. Chem. Phys.
Discussion started: 15 March 2017

PM_1 (sum of NR-PM_1 and BC) were comparable to those of $PM_{2.5}$ with a slope of 1.1 and Pearson correlation coefficient (R_p) of 0.95 (Fig. S2a) when using a CE of 0.7. Furthermore, total AMS organics were also correlated with organic matter (OM) concentrations derived from the OC measurements (Fig. S2b) with a slope of 1.1 and R_p of 0.82. The OC to OM conversion was calculated by organic matter to organic carbon ratio (OM:OC) data from the HR-ToF-AMS elemental analysis. AMS-measured sulfate, nitrate, and ammonium were comparable to those measured by MARGA with slopes of 1.0, 0.9, and 0.7, respectively. These comparisons supported a choice of CE = 0.7 is appropriate for the OA-dominating NR-PM_1 in this study.

Source apportionment for OA was performed by the newly developed ME-2 and controlled via the interface SoFi coded in Igor Pro (Canonaco et al., 2013). Fully unconstrained runs (PMF) were first explored. However, the three-factor solution suffers from mixing of factors of the HOA factor with the cooking organic aerosol (COA) factor (Fig. S3), as well as SVOOA with biomass burning related organic aerosol (BBOA) factor. The four-factor solution splits highly oxidized low-volatile OOA (LVOOA) into two sub-factors (Fig. S4). The inclusion of additional factors still cannot resolve pure primary OA factors (HOA, COA and BBOA), as they may have similar time series or profiles. Zhang et al. (2013) also reported that the PCA-resolved HOA might be affected by cooking emission with a distinct noontime peak in Beijing in spring and summer. The ME-2, however, by introducing *a priori* information of source profiles for HOA, COA and BBOA, provides additional control over the rotational ambiguity (Canonaco et al., 2013; Paatero and Hopke, 2009). The *a* value, ranging from zero to unity, stands for the percentage by which each m/z signal of the final solution spectra may differ from the anchor. A value of 0 means no deviation is allowed, while a value of 1 means 100% deviation is allowed. Several source profiles from previously reported HR-ToF-AMS data with different *a* values were explored. However, some ions were missing from the reference source profile when compared with our dataset. For these ions, the signal intensities were estimated based on the unit-mass-resolution (UMR) source profile from the average of multiple ambient data sets (Ng et al., 2011) as follows:

$$I_{m/z}=k*I_{UMR(m/z)}-I_{HRrest(m/z)} \quad (1);$$

$$k=I_{UMR(total)}/I_{HR(total)} \quad (2).$$

where $I_{m/z}$ is the signal intensity of the missing ions in the reference profile; k is a correction factor,

Atmos. Chem. Phys. Discuss., doi:10.5194/acp-2017-116, 2017
Manuscript under review for journal Atmos. Chem. Phys.
Discussion started: 15 March 2017

Atmospheric Chemistry and Physics Discussions

derived from the ratio of total signal intensities in the UMR and HR profiles, which accounts for the difference in total signal intensity between the profiles; $I_{UMR(m/z)}$ is the total signal intensity at UMR level for the missing ions in the UMR profile; and $I_{HRrest(m/z)}$ is the sum of the signal intensities of the rest of the ions from HR reference profile that shares the same integer m/z as the missing ions. For these ions, whose intensities are derived from the above equation, an *a* value of 1 (100% deviation) was used.

To tackle the problem of mixing of traffic and cooking source in our PMF runs, we used the ME-2 solver with reference HOA and COA mass spectra adopted from the Paris campaign (Crippa et al., 2013). The *a* values, ranging from 0 to 0.5 in increments of 0.1, were tested. However, the resolved-HOA factor contributed no more than 5% of total OA, and only exhibited a small morning rush peak in the diurnal pattern (Fig. S5). Furthermore, another factor was observed to share similar features with the HOA mass spectrum (Fig. S5). This factor exhibited clear rush-hour peaks during the morning and late afternoon, as with traffic-related pollutants (e.g. NO_x and BC). Also, the mass fraction of this factor is 3-4 times higher than the resolved-HOA factor (Fig. S5). The factor was observed, even with additional input for BBOA source profile and solutions with additional factors (Fig. S5) and continued to persist even after several HOA source profiles were tested. Alternatively, we directly extracted a local HOA source profile (HOA_{loc}) from the data set using a separate PMF run in selected time series with peaks in organic mass concentration. Similar approach has also been reported in by Fröhlich et al. (2015). We performed PMF on a short-term peak in the organic time series (Fig. S6) as well as on all of the short peaks with organic concentration above 30 μg/m^3 (Fig. S6). These two methods resolved similar mass spectra for local primary OA factors with R_{uc}=0.99 (Fig. S7a, S7b). The results remain the same with even more factors (Fig. S7c). We then used the HOA source profile obtained from all of the short peaks with organic concentration above 30 μg/m^3 (HOA_{local_2}) as the input HOA source profile. However, constrained HOA alone cannot resolved an environmentally reasonable solution either (Fig. S8). We then tried to added a COA constrain. For COA source profile, we compared the COA reference from the Paris campaign (Crippa et al., 2013) and the Mong Kok campaign in Hong Kong (Lee et al., 2015). When the two different COA source profiles were used in the ME-2 runs, similar COA (both in mass spectra and time series) were obtained for the current dataset (Fig. S9). The time series of the mass concentration of the COA factors tracked well with that of the COA tracer ion ($C_3H_3O^+$) and had clear mealtime peaks (Fig. S9). The ME-2 runs using these two COA source profiles differed

slightly in terms of the proportion of COA and LVOOA, with results using the COA profile from the Paris campaign yielding a lower concentration of COA and a higher concentration of LVOOA. The discrepancy was within 2 μg/m^3 (Fig. S9). As cooking styles and ingredients in Guangzhou are more similar to those in Hong Kong than in Paris, we chose the COA source profile from the Hong Kong campaign (HK) to constrain our ME-2 runs. For the BBOA factor, we used the reference BBOA profile from MILAGRO (Aiken et al., 2009). The resolved BBOA factor tracked well with its tracer ion ($C_2H_4O_2^+$) and potassium (K^+) in time series.

A four-factor (HOA, COA, BBOA and a free factor) solution had a higher Q/Q_{exp}, while a six-factor (HOA, COA, BBOA and three free factors) solution seemed to split OOA factors without obvious physical meaning. We first tried to explore the a value with the range of a values from 0 to 0.5. An five-factor solution with *a* values of 0.1, 0.2, 0.3 for HOA_{local}, COA_{HK}, and $BBOA_{MILAGRO}$, respectively, was finally adopted. The *a* values for these POA factors were also in line with previous ME-2 studies (Canonaco et al., 2013; Crippa et al., 2014; Fröhlich et al., 2015). We further run the ME-2 with the optimal conditions with 10 runs to explore the stability of solution. The time series and mass spectra for each runs were quite steady (Fig. S10). The final solution came from results obtained with averaging these ten runs. Two oxygenated organic aerosol factors, SVOOA and LVOOA, were assigned based on their degree of oxygenation. The mass spectra of all OA factors and their mass concentrations will be discussed in Section 2.2. The correlations of OA factors with external tracers are shown in Table S1.

3. Results and Discussion:

3.1. Overall composition

Fig. 1 shows the time series of NR-PM_1 species (sulfate, nitrate, ammonium, chloride, and organics), BC, and meteorological factors (precipitation, RH, temperature, wind direction, and wind speed) for the whole campaign. Northerly winds (hourly integrated) prevailed through the whole campaign, bringing pollutants from downtown area of Guangzhou. NO_x ranged from 9 to 333 ppb, averaging at 40.8 ppb. The high NO_x levels reflect heavy influences from traffic emissions. Ozone ranged from 0.2 to 119.9 ppb with an average of 22.7 ppb. An episodic high O_3 period occurred from the November 14th to 27th, 2014, and peaked in every afternoon. The average temperature was 5 °C lower in December than in November. A detailed discussion of the diurnal patterns of meteorological conditions together with gaseous and particulate pollutants is presented

in the supplementary information (Section 1). Mass concentrations of PM_1 ranged from 1.7 to 208.4 μg/m^3, with an average of 55.4 μg/m^3. The concentration was significantly higher than those in Hong Kong (Lee et al., 2013, 2015; Li et al., 2015; Qin et al., 2016a) and Shenzhen (He et al., 2011), similar with those in Lanzhou and Sichuan basin (Hu et al., 2016; Xu et al., 2016), and lower than those in Beijing (Hu et al., 2016) and Sichuan Basin. In our study, organics accounted for 24.5 μg/m^3 (or 46.3 %) of the PM_1 mass on average. Sulfate, nitrate, ammonium, BC, and chloride accounted for 23.1%, 11.2%, 9.1%, 8.3%, and 1.9% of the PM_1 mass, respectively (Fig. 2 a). Fig. 2b shows the variations in species mass fractions in PM_1 species as a function of total PM_1 (with BC inclusive) mass loading, as well as the probability density of PM_1 mass loading. Organic mass fraction was the highest across different PM_1 levels with little variation. On the contrary, the mass fraction of sulfate dropped from 0.25 to 0.15 as PM_1 concentration increased from 10 to 160 μg/m^3. The decrease in sulfate mass fraction was compensated by the increased mass fraction of nitrate, and to a lesser extent, chloride. The increase in the relative contribution of nitrate on highly polluted days was also observed in AMS studies in other locations in China, such as Shenzhen (He et al., 2011), Beijing (Huang et al., 2010), and Changdao (Hu et al., 2013).

3.2. Organics

Since OA accounted for over 45% of PM_1 in this study, it is worth investigating the detailed characteristics of this portion of PM. Elemental analysis of OA (ratios of H:C, O:C and OM:OC) provides useful information for assessing OA characteristics and their evolution. Ions in the high resolution mass spectra were used to calculate the elemental ratios using the Improved-Ambient method (Canagaratna et al., 2015). Results obtained from the Aiken-Ambient (Aiken et al., 2007) protocol were also listed in Table 1 for comparison with elemental ratios reported in the literature. We further used empirical constants (11% for H:C, 27% for O:C, and 9% for OM:OC) from Canagaratna et al. (2015) to estimate the ratios accounting for possible underestimation of the O:C ratio in earlier studies. As there are significant differences in O_x, RH and temperature between November and December, we conducted the following analysis in November and December separately. However, the average O:C, H:C, and OM:OC ratios showed little variation between the two months, with average values of 0.53 for O:C, 1.63 for H:C, 1.87 for OM:OC in November, and 0.53 for O:C, 1.65 for H:C and 1.87 for OM:OC in December. The observed elemental ratios generally agreed with other AMS-based reported values in PRD (Table 1). The H:C ratio was similar to those at rural sites in Kaiping (1.64) and Heshan (1.65) and slightly higher than that at

suburban HKUST (1.54 and 1.55) but lower than those at urban sites in Shenzhen (1.81) and Mong Kok (1.84). O:C and OM:OC ratios, on the contrary, are higher than those at the urban sites and lower than that in Kaiping, but similar to those in Heshan and at HKUST. Overall, the relatively low H:C ratio and high O:C ratio suggest that OA at this site has degree of oxygenation higher than those at urban sites (e.g. Shenzhen), but lower than those at rural sites (e.g. Kaiping). The degree of oxygenation reflects the characteristics of OA at the peripheries of urbanized areas as a mixture of background air with urban recently formed secondary OA.

As shown in Fig. 3, the diurnal variations in H:C, O:C, OM:OC and carbon oxidation state ($\overline{OS}_c \approx 2\times$O:C-H:C) showed similar patterns during both November and December. The average H:C ratio ranged from 1.6 to 1.7, with a pronounced increase in the late afternoon from 16:00 to 20:00, and remaining at a maximum value until mid-night. This observation suggests important fresh organic source at evening and nighttime. The O:C, OM:OC ratios and $\overline{OS}_c$ increased during daytime with afternoon peaks at around 15:00, likely due to high photochemical activity and production of SOA during daylight hours.

The mass spectra of all OA factors and their mass concentrations from PMF analysis with ME-2, together with the time series of external tracers, are shown in Fig. 4. HOA correlated well with NO_x since both are traffic-related species. While COA shares spectral similarities with HOA, it is distinguished from HOA by a higher contribution of $C_3H_3O^+$at m/z 55, and a much lower contribution of ions at m/z 57 compared to HOA (He et al., 2010; Mohr et al., 2012). The time series of the COA was highly correlated with one of its tracer ions, $C_3H_3O^+$. The other primary factor, BBOA, is characterized by the presence of signals at m/z 60 ($C_2H_4O_2^+$) and m/z 73 ($C_3H_5O_2^+$), which are typically associated with levoglucosan (Alfarra et al., 2007; Schneider et al., 2006). The time series of BBOA also tracked well with the one of its marker ions. The two oxygenated organic aerosol factors (SVOOA and LVOOA) are characterized by oxygenated ions $C_2H_3O^+$ at m/z 43 and CO_2^+ at m/z 44, respectively. The ratio of most oxidized ions CO_2^+ (m/z 44) to moderately oxygenated ions $C_2H_3O^+$ (m/z 43) is higher in LVOOA than that in SVOOA (Jimenez et al., 2009). Overall, a good correlation between the concentrations of SVOOA and nitrate, a semi-volatile secondary inorganic species, was observed. From 21st November to 1st December, SVOOA showed distinct peaks that are beyond the comparable trend with nitrate. The sharp peaks of SVOOA coincide with those of O_3 as shown in the inserted panel. Moreover, higher

temperatures were also observed during this period (Fig. 1). LVOOA also correlated well with sulfate in time series, as both species are regional pollutants. On average, HOA, SVOOA and LVOOA were the main sources of OA, made up 26%, 31% and 30% of the total OA respectively (Fig. 5).

The diurnal patterns of mass concentrations and fractions for the five OA factors are depicted in Fig. 6. HOA exhibited two typical peaks during both November and December, first during the morning rush hours at 09:00, before starting to increase again at 16:00 prior to peaking between 20:00 and mid-night. The high HOA level in the evening and at night was likely due to the heavily polluting trucks passing by en route to the downtown area at night (22:00 to 07:00). The diurnal variations in HOA corresponded to those in H:C ratio and NO_x, and BC (Fig. S11), suggesting that vehicle-related pollutants are the main contributor to this OA factor. On the other hand, COA had clear peaks at lunch and dinner times. Even though COA only contributed to 8% of total OA on average, its contribution could be as high as 15% of OA during mealtime in both months. Contribution of COA to OA at this peripheral site of the megacity Guangzhou, however, is still far lower than those directly measured at urban areas, which often had COA contribution of 15 – 20% of OA (Crippa et al., 2013; Lee et al., 2015; Sun et al., 2016, 2013). BBOA did not exhibit a clear diurnal variation in November, but it had a daytime valley in December, possibly due to intensive biomass burning activities at night. SVOOA had a clear noon-to-afternoon peak in November, consistent with peaks in ozone (Fig. S11), but this peak was less pronounced in December. The noon-to-afternoon peak for SVOOA has been commonly observed worldwide under the photochemically oxidation process (Hayes et al., 2013; Qin et al., 2016). Zotter et al. (2014) further found that the noon-to-afternoon SVOOA peak can be caused by the large increase in fossil carbon. LVOOA, in our study, showed a relatively flat diurnal pattern as in Shenzhen (He et al., 2011), but significant noon-to-afternoon peaks for LVOOA were observed at rural sites in Kaiping (Huang et al., 2011) and Hesan (Gong et al., 2012) .

3.3. Formation of SOA

The evolution of AMS OA factors has been used to infer SOA formation via photochemical oxidation in the PRD (Lee et al., 2013; Li et al., 2013; Qin et al., 2016a). Odd-oxygen (O_x) concentrations are closely linked to the extent of photochemical oxidation in an air mass because

O_3 production results from OH reactions with VOCs and CO. The ratio of SOA to O_x, therefore, provides a useful metric for quantifying the dependence of SOA concentration on photochemical oxidation. Following the work of Hayes et al. (2013), we examine the correlations of SOA with O_x, instead of O_3, to account for the titration of O_3 by freshly emitted NO, which produces NO_2. Fig. 7a shows that SOA (SVOOA+LVOOA) continuously increased as O_x increased during daytime (7:00 to 18:00) in both November and December. The regression slope for SOA versus O_x are 0.23 ±0.014 (R_{pr}=0.85) and 0.25 ±0.025 (R_{pr}=0.55) μg /(sm^3 ppb) in November and December, respectively. The volume unit "sm" stands for volume under standard-temperature-pressure conditions. The slopes are higher than those reported in earlier studies during spring to summer in North America (Table 2), indicating efficient SOA photochemical production even in late autumn and early winter at this subtropical site. Such a significant production of SOA might have been fueled by photo-oxidation of large amounts of accumulated VOCs between the city and this peripheral site of Guangzhou. Meteorological parameters can also influence the formation of SOA in several ways. Such influences can be effective by changing SOA partitioning at high temperature conditions, or promoting aqueous-phase chemistry at high liquid water content conditions. The temperature effect on gas-particle partitioning did not appear to be important in this study. Higher temperatures should favor the partitioning of SOA to the vapor phase, but higher SOA mass loading was associated with higher temperature in our case (Fig. 7b). In November, LWC stayed in a relatively narrow range (Fig. 7c) when SOA experienced the drastic changes. In December, LWC was lower than that in November, yet, SOA increased as LWC increased. The enhanced LWC may facilitate the SOA formation in December yet influence was not clear in November. Furthermore, there is no correlation between SOA/OA and LWC in either month.

3.4. Formation of nitrate

With the growth of NO_x emissions in recent years, the concentration and proportions of nitrate in PM have increased significantly in most Chinese megacities (Pan et al., 2016; Wen et al., 2015; Xue et al., 2014). As shown in Fig. 2, an obvious increased proportion of nitrate was also observed in high-PM episodes in our study. The increased contribution of nitrate to PM calls for a more detailed investigation of this species.

We used molar concentration of total nitrate [HNO_3(g) + NO_3^-(p)] to examine the increase of nitrate species, where HNO_3(g) was measured with MARGA and NO_3^-(p) was measured with HR-

Atmos. Chem. Phys. Discuss., doi:10.5194/acp-2017-116, 2017
Manuscript under review for journal Atmos. Chem. Phys.
Discussion started: 15 March 2017

ToF-AMS. Organic nitrates may show similar fragments (NO^+ and NO_2^+) with inorganic nitrate in HR-ToF-AMS and contribute to the nitrate concentration measured by AMS. Farmer et al. (2010) have successfully used NO^+ to NO_2^+ ratio to estimate organic nitrates from HR-ToF-AMS measurement. The rationale behind such an estimation was that the response of NO^+/NO_2^+ of inorganic nitrate differed greatly those from organic nitrates. Xu et al.(2015) used the NO^+/NO_2^+ values of 5 and 10, which likely correspond to the upper and lower bounds of the ratios from organic nitrates. This method using NO^+/NO_2^+ (Method 1) was adopted in this study to estimate the contributions of inorganic and organic nitrates. However, it should be noted that the vast array of possible organic nitrate parent compounds in ambient particles and the variations of the NO^+/NO_2^+ ratios between instruments may led to some bias in the calculation. A lower bound of organic nitrate concentration can also be estimated using the organic concentration and elemental ratios (OM:OC and N:C) from HR-ToF-AMS measurement (Method 2) (Schurman et al., 2015b). A detailed calculation of the two methods is presented in the supplemental information (Text S2). Using these two methods, the estimated inorganic nitrate concentrations were derived by subtracting the contributions of organic nitrates from the total nitrate as measured by the HR-ToF-AMS. Overall, the contribution from organic nitrate ranged from around 10% to 25%, while inorganic nitrate contributed to the majority signals of AMS-measured nitrate. The scatter plot of estimated inorganic nitrate versa nitrate from HR-ToF-AMS measurement is shown in Fig. 8. The estimated inorganic nitrate tracked well ($R_p^2 \geq 0.95$) with the total HR-ToF-AMS nitrate concentration and followed with the 1 to 1 line. Even though organic nitrates also contributed to the total nitrate we measured, both the variation and the concentration of the nitrate did not change significantly after subtracting the organic nitrates. Furthermore, as shown in Fig. S2, concentrations of nitrate from AMS were comparable to those from MAGRA, which uses chromatographic speciation, with a correlation slope of 0.9 and a R_p of 0.95. The influence from organic nitrates in our calculation of total nitrate should be minor. Given the uncertainties associated with each estimation, we prefer to use the raw HR-ToF-AMS nitrate concentration in the following discussion. In Fig. 9, the total nitrate is closely correlated with NO_x during both daytime and nighttime. At the same NO_x, total nitrate increased as O_x increased during daytime, suggesting that NO_x was photochemically oxidized to nitrate species. At night (Fig. 9b), O_x concentration was relatively low when NO_x concentrations were high. The slope of total nitrate against NO_x during daytime is steeper than that at nighttime. Nighttime formation of nitric acid

involves the consumption of NO_x and O_3 (Seinfeld and Pandis, 2006). While NO_x can be replenished by primary emissions, O_3 is mainly produced during daytime and is consumed at night. Thus, it is reasonable to observe that high total nitrate concentration was correlated with high NO_x and low O_3 at night.

The formation of particulate nitrate is limited by the availability of ammonia. Gas-to-particle partitioning of nitrate species to form particulate nitrate can be affected by the concentrations of ammonium and sulfate. An increase in ammonium or a decrease in sulfate could enhance the formation of particulate nitrate (Seinfeld and Pandis, 2006). Many studies indicated that the molar ratio of ammonium to sulfate of 1.5 demarcates the observation of particulate nitrate (Pathak et al., 2004, Griffith et al., 2015; Liu et al., 2015). Under ammonium rich (AR, $[NH_4^+]/[SO_4^{2-}] > 1.5$) conditions, additional ammonia is available to transfer HNO_3 to the particle phase. In contrast, under (AP, $[NH_4^+]/[SO_4^{2-}] < 1.5$) conditions, all of the ammonia is used to neutralize H_2SO_4 until $(NH_4)_3H(SO_4)_2$ (letovicite) is formed. AR conditions prevailed during the whole campaign. Excess ammonium, defined as ($[NH_4^+]/[SO_4^{2-}]$ - 1.5) × $[SO_4^{2-}]$), tracked well with particulate nitrate concentration with a slope of 0.93 (Fig. 10). In Fig. 11, we also examined the relationship between nitrate in $PM_{2.5}$ and excess ammonium, and alkali cations (Na^+ and Ca^{2+}, mainly from soil dust and sea salt particles, respectively). Results showed that nitrate tracked better with excess ammonium than the alkali cations did. The slope of nitrate to excess ammonium was smaller than 1, indicating that ammonium was sufficient to neutralize the particulate nitrate. The molar concentration of alkali cations was around 7-10 times lower than that of nitrate and their role in stabilizing nitrate was negligible in our study.

The partitioning of nitrate between the gas and particle phases shows significant differences between November and December (data points in Fig. 12). The average ratio of nitrate to HNO_3 (the slope of scatter plot) was 3.2 in November, compared to 7.8 in December. The NH_3 concentration in the gas phase was not a limiting factor as the concentration of NH_3 was even higher in November (Fig. 11a). Lower temperatures in December shifted the equilibrium toward the particle phase, increasing the nitrate concentration in the particle phase (Fig. 12b). Higher RH or particle liquid water content favored the thermodynamic equilibrium to form particulate nitrate. However, this effect fails to explain the gap between the different months (Fig. 12 c,d) as the higher nitrate to HNO_3 ratio (December data) was associated with the lower RH and LWC. Overall, the differences in the ambient temperature may be the key factor causing the large difference in

gas-particle partitioning of nitrate in different time of a year. The implication for this finding is that meteorological parameters might couple with chemistry in the formation of PM species such as the semi-volatile nitrate. As such, the complex effects in PM formation deserve further investigations, especially in city peripheries where precursors are abundant and photochemistry is active.

4. Conclusions

This study presents the emission sources and formation routes of PM at Panyu District in peripheral Guangzhou, from November to December 2014. The measured PM_1 (sum of NR-PM_1 and BC) mass concentration ranged from 1.7 to 208.4 μg/m^3, with an average of 55.4 μg/m^3. The PM_1 concentration is high compared to other cities in PRD, but slightly lower than those in the northern and north-western parts of China. OA was the overwhelmingly dominate species (> 45%) at all PM_1 levels. The mass fraction of sulfate decreased from 0.25 to 0.15 as PM_1 concentration increased from 10 to 160 μg/m^3. The decrease in sulfate mass fraction was compensated by the increased mass fraction of nitrate. For organics, the average H:C ratio showed a pronounced increase starting in late afternoon and lasting until mid-night, suggesting the presence of an important fresh OA source at nighttime in peripheral Guangzhou, most likely heavy-duty diesel trucks. The O:C and OM:OC ratios, as well as $\overline{OS}_c$ increased during daytime with clear afternoon peaks, likely due to efficient photochemical production of SOA during daytime. OA components were resolved by PMF analysis with ME-2. Fully unconstrained runs (PMF) suffers from the mixing of factors of the HOA factor with the COA factor, as well as the SVOOA) with the BBOA factor. A systematic approach to minimize the mixing of factors is explored. The final resolved components are HOA, COA, BBOA, SVOOA, and LVOOA. Results show that HOA was an important contributor (40%) to the high organic concentrations at night. SOA (SVOOA+LVOOA) plays a more important role during daytime. SOA concentration changed with the photochemical oxidation marker (O_x). More interestingly, the ratios of SOA to O_x during the late autumn and early wintertime were higher than those reported for several urban sites in North American during the summer (e.g. Pasadena and Mexico City), indicating the efficient SOA production. This efficient SOA formation was probably a result of active photochemistry at this subtropical site and was fueled by the large source of SOA precursors (e.g. HOA and VOCs) in the periphery of Guangzhou. The formation of total nitrate was closely correlated with NO_x during both nighttime

and daytime, again demonstrating a close tie to traffic emissions at this site peripheral to the megacity. However, the slope of total nitrate against NO_x at daytime is steeper than that at nighttime. During daytime, at the same NO_x level, total nitrate increased as O_x increased, suggesting that NO_x photochemically oxidizes to nitrate. At night, high total nitrate concentration was associated with high NO_x but low O_x. Ammonium-rich conditions prevailed throughout the whole campaign and particulate nitrate was highly associated with the excess ammonium. The fraction of nitrate in the particulate phase out of total nitrate is higher in December, primarily due to difference in temperature. Nevertheless, in addition to its close tie to traffic emissions (NO_x as the precursors), formation of particulate nitrate may be affected by meteorological parameters as well. This study underlines the effects of traffic emissions to peripheral Guangzhou. The contributions to PM can be direct contribution of primary OA (HOA), secondary formation of semi-volatile OA (SVOOA), as well as secondary formation and subsequent partitioning of nitrate during late autumn and early winter.

5. Acknowledgements:

This work was supported by the National Key Project of the Ministry of Science and Technology of the People's Republic of China (2016YFC0201901) and the Natural Science Foundation of China (41375156). We also thank Dr. Mai Boru for providing CO_2 data. Yi Ming Qin gratefully acknowledges support from the HKUST Asian Future Leaders Scholarship.

6. Reference:

Aiken, A. C., DeCarlo, P. F. and Jimenez, J. L.: Elemental analysis of organic species with electron ionization high-resolution mass spectrometry., Anal. Chem., 79(21), 8350–8, doi:10.1021/ac071150w, 2007.

Aiken, A. C., Salcedo, D., Cubison, M. J., Huffman, J. A., DeCarlo, P. F., Ulbrich, I. M., Docherty, K. S., Sueper, D., Kimmel, J. R., Worsnop, D. R., Trimborn, A., Northway, M., Stone, E. A., Schauer, J. J., Volkamer, R. M., Fortner, E., de Foy, B., Wang, J., Laskin, A., Shutthanandan, V., Zheng, J., Zhang, R., Gaffney, J., Marley, N. A., Paredes-Miranda, G., Arnott, W. P., Molina, L. T., Sosa, G. and Jimenez, J. L.: Mexico City aerosol analysis during MILAGRO using high resolution aerosol mass spectrometry at the urban supersite (T0) – Part 1: Fine particle composition and organic source apportionment, Atmos. Chem. Phys., 9(17), 6633–6653, doi:10.5194/acp-9-6633-2009, 2009.

Alfarra, M. R., Prevot, A. S. H., Szidat, S., Sandradewi, J., Weimer, S., Lanz, V. A., Schreiber, D., Martin Mohr, A. and Urs, B.: Identification of the Mass Spectral Signature of Organic Aerosols from Wood Burning Emissions, , doi:10.1021/ES062289B, 2007.

Canagaratna, M. R., Jimenez, J. L., Kroll, J. H., Chen, Q., Kessler, S. H., Massoli, P., Hildebrandt Ruiz, L., Fortner, E., Williams, L. R., Wilson, K. R., Surratt, J. D., Donahue, N. M., Jayne, J. T. and Worsnop, D. R.: Elemental ratio measurements of organic compounds using aerosol mass spectrometry: characterization, improved calibration, and implications, Atmos. Chem. Phys., 15(1), 253–272, doi:10.5194/acp-15-253-2015, 2015.

Canonaco, F., Crippa, M., Slowik, J. G., Baltensperger, U. and Prévôt, A. S. H.: SoFi, an IGOR-based interface for the efficient use of the generalized multilinear engine (ME-2) for the source apportionment: ME-2 application to aerosol mass spectrometer data, Atmos. Meas. Tech., 6(12), 3649–3661, doi:10.5194/amt-6-3649-2013, 2013.

Chan, C. K. and Yao, X.: Air pollution in mega cities in China, Atmos. Environ., 42(1), 1–42, doi:10.1016/j.atmosenv.2007.09.003, 2008.

Clegg, S. L., Brimblecombe, P. and Wexler, A. S.: Thermodynamic Model of the System $H^{+}-NH_{4}^{+}-Na^{+}-SO_{4}^{2-}-NO_{3}^{-}-Cl^{-}-H_{2}O$ at 298.15 K, J. Phys. Chem. A, 102(12), 2155–2171, doi:10.1021/jp973043j, 1998.

Crippa, M., El Haddad, I., Slowik, J. G., DeCarlo, P. F., Mohr, C., Heringa, M. F., Chirico, R., Marchand, N., Sciare, J., Baltensperger, U. and Prévôt, A. S. H.: Identification of marine and continental aerosol sources in Paris using high resolution aerosol mass spectrometry, J. Geophys. Res. Atmos., 118(4), 1950–1963, doi:10.1002/jgrd.50151, 2013.

Crippa, M., Canonaco, F., Lanz, V. A., Äijälä, M., Allan, J. D., Carbone, S., Capes, G., Ceburnis, D., Dall'Osto, M., Day, D. A., DeCarlo, P. F., Ehn, M., Eriksson, A., Freney, E., Hildebrandt Ruiz, L., Hillamo, R., Jimenez, J. L., Junninen, H., Kiendler-Scharr, A., Kortelainen, A.-M., Kulmala, M., Laaksonen, A., Mensah, A. A., Mohr, C., Nemitz, E., O'Dowd, C., Ovadnevaite, J., Pandis, S. N., Petäjä, T., Poulain, L., Saarikoski, S., Sellegri, K., Swietlicki, E., Tiitta, P., Worsnop, D. R., Baltensperger, U. and Prévôt, A. S. H.: Organic aerosol components derived from 25 AMS data sets across Europe using a consistent ME-2 based source apportionment approach, Atmos. Chem. Phys., 14(12), 6159–6176, doi:10.5194/acp-14-6159-2014, 2014.

Decarlo, P. F., Kimmel, J. R., Trimborn, A., Northway, M. J., Jayne, J. T., Aiken, A. C., Gonin, M., Fuhrer, K., Horvath, T., Docherty, K. S., Worsnop, D. R. and Jimenez, J. L.: Field-Deployable, High-Resolution, Time-of-Flight Aerosol Mass Spectrometer, Anal. Chem., 78(24), 8281–8289, doi:8410.1029/2001JD001213.Analytical, 2006.

Docherty, K. S., Aiken, A. C., Huffman, J. A., Ulbrich, I. M., Decarlo, P. F., Sueper, D., Worsnop,

D. R., Snyder, D. C., Peltier, R. E., Weber, R. J., Grover, B. D., Eatough, D. J., Williams, B. J., Goldstein, A. H., Ziemann, P. J. and Jimenez, J. L.: The 2005 Study of Organic Aerosols at Riverside (SOAR-1): Instrumental intercomparisons and fine particle composition, Atmos. Chem. Phys., 11(23), 12387–12420, doi:10.5194/acp-11-12387-2011, 2011.

Drinovec, L., Močnik, G., Zotter, P., Prévôt, A. S. H., Ruckstuhl, C., Coz, E., Rupakheti, M., Sciare, J., Müller, T., Wiedensohler, A. and Hansen, A. D. A.: The "dual-spot" Aethalometer: An improved measurement of aerosol black carbon with real-time loading compensation, Atmos. Meas. Tech., 8(5), 1965–1979, doi:10.5194/amt-8-1965-2015, 2015.

Elser, M., Huang, R.-J., Wolf, R., Slowik, J. G., Wang, Q., Canonaco, F., Li, G., Bozzetti, C., Daellenbach, K. R., Huang, Y., Zhang, R., Li, Z., Cao, J., Baltensperger, U., El-Haddad, I. and Prévôt, A. S. H.: New insights into PM_{2.5} chemical composition and sources in two major cities in China during extreme haze events using aerosol mass spectrometry, Atmos. Chem. Phys., 16(5), 3207–3225, doi:10.5194/acp-16-3207-2016, 2016.

Farmer, D. K., Matsunaga, a, Docherty, K. S., Surratt, J. D., Seinfeld, J. H., Ziemann, P. J. and Jimenez, J. L.: Response of an aerosol mass spectrometer to organonitrates and organosulfates and implications for atmospheric chemistry., Proc. Natl. Acad. Sci. U. S. A., 107(15), 6670–6675, doi:10.1073/pnas.0912340107, 2010.

Fröhlich, R., Crenn, V., Setyan, A., Belis, C. A., Canonaco, F., Favez, O., Riffault, V., Slowik, J. G., Aas, W., Aijälä, M., Alastuey, A., Artiñano, B., Bonnaire, N., Bozzetti, C., Bressi, M., Carbone, C., Coz, E., Croteau, P. L., Cubison, M. J., Esser-Gietl, J. K., Green, D. C., Gros, V., Heikkinen, L., Herrmann, H., Jayne, J. T., Lunder, C. R., Minguillón, M. C., Močnik, G., O'Dowd, C. D., Ovadnevaite, J., Petralia, E., Poulain, L., Priestman, M., Ripoll, A., Sarda-Estève, R., Wiedensohler, A., Baltensperger, U., Sciare, J. and Prévôt, A. S. H.: ACTRIS ACSM intercomparison – Part 2: Intercomparison of ME-2 organic source apportionment results from 15 individual, co-located aerosol mass spectrometers, Atmos. Meas. Tech., 8(6), 2555–2576, doi:10.5194/amt-8-2555-2015, 2015.

Gong, Z., Lan, Z., Xue, L., Zeng, L., He, L. and Huang, X.: Characterization of submicron aerosols in the urban outflow of the central Pearl River Delta region of China, Front. Environ. Sci. Eng. China, 6(5), 725–733, doi:10.1007/s11783-012-0441-8, 2012.

Griffith, S. M., Huang, X. H. H. H., Louie, P. K. K. K. K. and Yu, J. Z.: Characterizing the thermodynamic and chemical composition factors controlling PM2.5 nitrate: Insights gained from two years of online measurements in Hong Kong, Atmos. Environ., 122, 864–875, doi:10.1016/j.atmosenv.2015.02.009, 2015.

Hagler, G. S. W., Bergin, M. H., Salmon, L. G., Yu, J. Z., Wan, E. C. H., Zheng, M., Zeng, L. M., Kiang, C. S., Zhang, Y. H., Lau, A. K. H. and Schauer, J. J.: Source areas and chemical composition of fine particulate matter in the Pearl River Delta region of China, Atmos. Environ., 40(20), 3802–3815, doi:10.1016/j.atmosenv.2006.02.032, 2006.

Hallquist, M., Wenger, J. C., Baltensperger, U., Rudich, Y., Simpson, D., Claeys, M., Dommen, J., Donahue, N. M., George, C., Goldstein, a. H., Hamilton, J. F., Herrmann, H., Hoffmann, T., Iinuma, Y., Jang, M., Jenkin, M. E., Jimenez, J. L., Kiendler-Scharr, a., Maenhaut, W., McFiggans, G., Mentel, T. F., Monod, a., Prévôt, a. S. H., Seinfeld, J. H., Surratt, J. D., Szmigielski, R. and Wildt, J.: The formation, properties and impact of secondary organic aerosol: current and emerging issues, Atmos. Chem. Phys., 9(14), 5155–5236, doi:10.5194/acp-9-5155-2009, 2009.

Hayes, P. L., Ortega, a. M., Cubison, M. J., Froyd, K. D., Zhao, Y., Cliff, S. S., Hu, W. W., Toohey, D. W., Flynn, J. H., Lefer, B. L., Grossberg, N., Alvarez, S., Rappenglück, B., Taylor, J. W., Allan, J. D., Holloway, J. S., Gilman, J. B., Kuster, W. C., De Gouw, J. a., Massoli, P., Zhang, X., Liu,

J., Weber, R. J., Corrigan, a. L., Russell, L. M., Isaacman, G., Worton, D. R., Kreisberg, N. M., Goldstein, a. H., Thalman, R., Waxman, E. M., Volkamer, R., Lin, Y. H., Surratt, J. D., Kleindienst, T. E., Offenberg, J. H., Dusanter, S., Griffith, S., Stevens, P. S., Brioude, J., Angevine, W. M. and Jimenez, J. L.: Organic aerosol composition and sources in Pasadena, California, during the 2010 CalNex campaign, J. Geophys. Res. Atmos., 118(16), 9233–9257, doi:10.1002/jgrd.50530, 2013.

He, L.-Y., Huang, X.-F., Xue, L., Hu, M., Lin, Y., Zheng, J., Zhang, R. and Zhang, Y.-H.: Submicron aerosol analysis and organic source apportionment in an urban atmosphere in Pearl River Delta of China using high-resolution aerosol mass spectrometry, J. Geophys. Res., 116(D12), D12304, doi:10.1029/2010JD014566, 2011.

He, L. Y., Lin, Y., Huang, X. F., Guo, S., Xue, L., Su, Q., Hu, M., Luan, S. J. and Zhang, Y. H.: Characterization of high-resolution aerosol mass spectra of primary organic aerosol emissions from Chinese cooking and biomass burning, Atmos. Chem. Phys., 10(23), 11535–11543, doi:10.5194/acp-10-11535-2010, 2010.

Ho, K. ., Lee, S. ., Chan, C. K., Yu, J. C., Chow, J. C. and Yao, X. .: Characterization of chemical species in PM2.5 and PM10 aerosols in Hong Kong, Atmos. Environ., 37(1), 31–39, doi:10.1016/S1352-2310(02)00804-X, 2003.

Hu, W., Hu, M., Hu, W.-W., Niu, H., Zheng, J., Wu, Y., Chen, W., Chen, C., Li, L., Shao, M., Xie, S. and Zhang, Y.: Characterization of submicron aerosols influenced by biomass burning at a site in the Sichuan Basin, southwestern China, Atmos. Chem. Phys., 16(20), 13213–13230, doi:10.5194/acp-16-13213-2016, 2016a.

Hu, W., Hu, M., Hu, W., Jimenez, J. L., Yuan, B., Chen, W., Wang, M., Wu, Y., Chen, C., Wang, Z., Peng, J., Zeng, L. and Shao, M.: Chemical composition, sources, and aging process of submicron aerosols in Beijing: Contrast between summer and winter, J. Geophys. Res. Atmos., 121(4), 1955–1977, doi:10.1002/2015JD024020, 2016b.

Hu, W. W., Hu, M., Yuan, B., Jimenez, J. L., Tang, Q., Peng, J. F., Hu, W. W., Shao, M., Wang, M., Zeng, L. M., Wu, Y. S., Gong, Z. H., Huang, X. F. and He, L. Y.: Insights on organic aerosol aging and the influence of coal combustion at a regional receptor site of central eastern China, Atmos. Chem. Phys., 13(19), 10095–10112, doi:10.5194/acp-13-10095-2013, 2013.

Huang, X., He, L., Hu, M., Canagaratna, M. R., Sun, Y., Zhang, Q., Zhu, T., Xue, L., Zeng, L. and Liu, X.: and Physics Highly time-resolved chemical characterization of atmospheric submicron particles during 2008 Beijing Olympic Games using an Aerodyne High-Resolution Aerosol Mass Spectrometer, , 8933–8945, doi:10.5194/acp-10-8933-2010, 2010.

Huang, X.-F. F., He, L.-Y. Y., Hu, M., Canagaratna, M. R., Kroll, J. H., Ng, N. L., Zhang, Y.-H. H., Lin, Y., Xue, L., Sun, T.-L. L., Liu, X.-G. G., Shao, M., Jayne, J. T. and Worsnop, D. R.: Characterization of submicron aerosols at a rural site in Pearl River Delta of China using an Aerodyne High-Resolution Aerosol Mass Spectrometer, Atmos. Chem. Phys., 11(5), 1865–1877, doi:10.5194/acp-11-1865-2011, 2011.

Huang, X. F., Yu, J. Z., He, L. Y. and Yuan, Z.: Water-soluble organic carbon and oxalate in aerosols at a coastal urban site in China: Size distribution characteristics, sources, and formation mechanisms, J. Geophys. Res. Atmos., 111(22), 1–11, doi:10.1029/2006JD007408, 2006.

Jimenez, J. L., Canagaratna, M. R., Donahue, N. M., Prevot, a S. H., Zhang, Q., Kroll, J. H., DeCarlo, P. F., Allan, J. D., Coe, H., Ng, N. L., Aiken, a C., Docherty, K. S., Ulbrich, I. M., Grieshop, a P., Robinson, a L., Duplissy, J., Smith, J. D., Wilson, K. R., Lanz, V. a, Hueglin, C., Sun, Y. L., Tian, J., Laaksonen, a, Raatikainen, T., Rautiainen, J., Vaattovaara, P., Ehn, M., Kulmala, M., Tomlinson, J. M., Collins, D. R., Cubison, M. J., Dunlea, E. J., Huffman, J. a, Onasch,

T. B., Alfarra, M. R., Williams, P. I., Bower, K., Kondo, Y., Schneider, J., Drewnick, F., Borrmann, S., Weimer, S., Demerjian, K., Salcedo, D., Cottrell, L., Griffin, R., Takami, a, Miyoshi, T., Hatakeyama, S., Shimono, a, Sun, J. Y., Zhang, Y. M., Dzepina, K., Kimmel, J. R., Sueper, D., Jayne, J. T., Herndon, S. C., Trimborn, a M., Williams, L. R., Wood, E. C., Middlebrook, a M., Kolb, C. E., Baltensperger, U. and Worsnop, D. R.: Evolution of organic aerosols in the atmosphere., Science, 326(5959), 1525–1529, doi:10.1126/science.1180353, 2009.

Lee, B. P., Li, Y. J., Yu, J. Z., Louie, P. K. K. and Chan, C. K.: Physical and chemical characterization of ambient aerosol by HR-ToF-AMS at a suburban site in Hong Kong during springtime 2011, J. Geophys. Res. Atmos., 118(15), 8625–8639, doi:10.1002/jgrd.50658, 2013.

Lee, B. P., Li, Y. J., Yu, J. Z., Louie, P. K. K. and Chan, C. K.: Journal of Geophysical Research : Atmospheres, , 1–19, doi:10.1002/2015JD023311.Received, 2015.

Li, Y. J., Lee, B. Y. L., Yu, J. Z., Ng, N. L. and Chan, C. K.: Evaluating the degree of oxygenation of organic aerosol during foggy and hazy days in Hong Kong using high-resolution time-of-flight aerosol mass spectrometry (HR-ToF-AMS), Atmos. Chem. Phys., 13(17), 8739–8753, doi:10.5194/acp-13-8739-2013, 2013.

Li, Y. J., Lee, B. P., Su, L., Fung, J. C. H. and Chan, C. K.: Seasonal characteristics of fine particulate matter (PM) based on high-resolution time-of-flight aerosol mass spectrometric (HR-ToF-AMS) measurements at the HKUST Supersite in Hong Kong, Atmos. Chem. Phys., 15(1), 37–53, doi:10.5194/acp-15-37-2015, 2015.

Liu, X., Sun, K., Qu, Y., Hu, M., Sun, Y., Zhang, F. and Zhang, Y.: Secondary formation of sulfate and nitrate during a haze episode in megacity beijing, china, Aerosol Air Qual. Res., 15(6), 2246–2257, doi:10.4209/aaqr.2014.12.0321, 2015.

Louie, P. K. K., Chow, J. C., Chen, L. W. A., Watson, J. G., Leung, G. and Sin, D. W. M.: PM2.5 chemical composition in Hong Kong: Urban and regional variations, Sci. Total Environ., 338(3), 267–281, doi:10.1016/j.scitotenv.2004.07.021, 2005.

Lu, Z., Streets, D. G., Zhang, Q., Wang, S., Carmichael, G. R., Cheng, Y. F., Wei, C., Chin, M., Diehl, T. and Tan, Q.: Sulfur dioxide emissions in China and sulfur trends in East Asia since 2000, Atmos. Chem. Phys., 10(13), 6311–6331, doi:10.5194/acp-10-6311-2010, 2010.

Mohr, C., DeCarlo, P. F., Heringa, M. F., Chirico, R., Slowik, J. G., Richter, R., Reche, C., Alastuey, A., Querol, X., Seco, R., Peñuelas, J., Jiménez, J. L., Crippa, M., Zimmermann, R., Baltensperger, U. and Prévôt, A. S. H.: Identification and quantification of organic aerosol from cooking and other sources in Barcelona using aerosol mass spectrometer data, Atmos. Chem. Phys., 12(4), 1649–1665, doi:10.5194/acp-12-1649-2012, 2012.

Ng, N. L., Canagaratna, M. R., Jimenez, J. L., Zhang, Q., Ulbrich, I. M. and Worsnop, D. R.: Real-time methods for estimating organic component mass concentrations from aerosol mass spectrometer data, Environ. Sci. Technol., 45(3), 910–916, doi:10.1021/es102951k, 2011.

Paatero, P. and Hopke, P. K.: Rotational tools for factor analytic models, J. Chemom., 23(2), 91–100, doi:10.1002/cem.1197, 2009.

Pan, Y., Wang, Y., Zhang, J., Liu, Z., Wang, L., Tian, S., Tang, G., Gao, W., Ji, D., Song, T. and Wang, Y.: Redefining the importance of nitrate during haze pollution to help optimize an emission control strategy., 2016.

Pathak, R. K., Louie, P. K. K. and Chan, C. K.: Characteristics of aerosol acidity in Hong Kong, Atmos. Environ., 38(19), 2965–2974, doi:10.1016/j.atmosenv.2004.02.044, 2004.

Qin, Y. M., Li, Y. J., Wang, H., Lee, B. P. Y. L., Huang, D. D. and Chan, C. K.: Particulate matter (PM) episodes at a suburban site in Hong Kong: evolution of PM characteristics and role of photochemistry in secondary aerosol formation, Atmos. Chem. Phys., 16(11), 14131–14145,

doi:10.5194/acp-2016-414, 2016a.
Qin, Y. M., Li, Y. J., Wang, H., Lee, B. P. Y. L., Huang, D. D. and Chan, C. K.: Particulate matter (PM) episodes at a suburban site in Hong Kong: evolution of PM characteristics and role of photochemistry in secondary aerosol formation, Atmos. Chem. Phys. Discuss., 0, 1–32, doi:10.5194/acp-2016-414, 2016b.
Schneider, J., Weimer, S., Drewnick, F., Borrmann, S., Helas, G., Gwaze, P., Schmid, O., Andreae, M. O. and Kirchner, U.: Mass spectrometric analysis and aerodynamic properties of various types of combustion-related aerosol particles, Int. J. Mass Spectrom., 258(1–3), 37–49, doi:10.1016/j.ijms.2006.07.008, 2006.
Schurman, M. I., Lee, T., Sun, Y., Schichtel, B. A., Kreidenweis, S. M. and Collett Jr., J. L.: Investigating types and sources of organic aerosol in Rocky Mountain National Park using aerosol mass spectrometry, Atmos. Chem. Phys., 15(2), 737–752, doi:10.5194/acp-15-737-2015, 2015a.
Schurman, M. I., Lee, T., Desyaterik, Y., Schichtel, B. A., Kreidenweis, S. M. and Collett, J. L.: Transport, biomass burning, and in-situ formation contribute to fine particle concentrations at a remote site near Grand Teton National Park, Atmos. Environ., 112, 257–268, doi:10.1016/j.atmosenv.2015.04.043, 2015b.
Seinfeld, J. H. and Pandis, S. N.: ATMOSPHERIC From Air Pollution to Climate Change SECOND EDITION., 2006.
Sun, C., Lee, B. P., Huang, D., Jie Li, Y., Schurman, M. I., Louie, P. K. K., Luk, C. and Chan, C. K.: Continuous measurements at the urban roadside in an Asian megacity by Aerosol Chemical Speciation Monitor (ACSM): particulate matter characteristics during fall and winter seasons in Hong Kong, Atmos. Chem. Phys., 16(3), 1713–1728, doi:10.5194/acp-16-1713-2016, 2016.
Sun, Y. L., Zhang, Q., Schwab, J. J., Demerjian, K. L., Chen, W. N., Bae, M. S., Hung, H. M., Hogrefe, O., Frank, B., Rattigan, O. V. and Lin, Y. C.: Characterization of the sources and processes of organic and inorganic aerosols in New York city with a high-resolution time-of-flight aerosol mass apectrometer, Atmos. Chem. Phys., 11(4), 1581–1602, doi:10.5194/acp-11-1581-2011, 2011.
Sun, Y. L., Wang, Z. F., Fu, P. Q., Yang, T., Jiang, Q., Dong, H. B., Li, J. and Jia, J. J.: Aerosol composition, sources and processes during wintertime in Beijing, China, Atmos. Chem. Phys., 13(9), 4577–4592, doi:10.5194/acp-13-4577-2013, 2013.
Tan, H., Yin, Y., Gu, X., Li, F., Chan, P. W., Xu, H., Deng, X. and Wan, Q.: An observational study of the hygroscopic properties of aerosols over the Pearl River Delta region, Atmos. Environ., 77, 817–826, doi:10.1016/j.atmosenv.2013.05.049, 2013.
Wang, Y., Zhang, Q. Q., He, K., Zhang, Q. and Chai, L.: Sulfate-nitrate-ammonium aerosols over China: Response to 2000-2015 emission changes of sulfur dioxide, nitrogen oxides, and ammonia, Atmos. Chem. Phys., 13(5), 2635–2652, doi:10.5194/acp-13-2635-2013, 2013.
Wen, L., Chen, J., Yang, L., Wang, X., Xu, C., Sui, X., Yao, L., Zhu, Y., Zhang, J., Zhu, T. and Wang, W.: Enhanced formation of fine particulate nitrate at a rural site on the North China Plain in summer: The important roles of ammonia and ozone, Atmos. Environ., 101, 294–302, doi:10.1016/j.atmosenv.2014.11.037, 2015.
Wu, X., Wu, Y., Zhang, S., Liu, H., Fu, L. and Hao, J.: Assessment of vehicle emission programs in China during 1998-2013: Achievement, challenges and implications, Environ. Pollut., 214(X), 556–567, doi:10.1016/j.envpol.2016.04.042, 2016.
Xu, J., Shi, J., Zhang, Q., Ge, X., Canonaco, F., Prévôt, A. S. H., Vonwiller, M., Szidat, S., Ge, J., Ma, J., An, Y., Kang, S. and Qin, D.: Wintertime organic and inorganic aerosols in Lanzhou, China: sources, processes, and comparison with the results during summer, Atmos. Chem. Phys, 16,

14937–14957, doi:10.5194/acp-16-14937-2016, 2016.

Xu, L., Suresh, S., Guo, H., Weber, R. J. and Ng, N. L.: Aerosol characterization over the southeastern United States using high-resolution aerosol mass spectrometry: spatial and seasonal variation of aerosol composition and sources with a focus on organic nitrates, Atmos. Chem. Phys., 15(13), 7307–7336, doi:10.5194/acp-15-7307-2015, 2015.

Xue, J., Yuan, Z., Lau, A. K. H. and Yu, J. Z.: Insights into factors affecting nitrate in $PM_{2.5}$ in a polluted high NO_x environment through hourly observations and size distribution measurements, J. Geophys. Res. Atmos., 119(8), 4888–4902, doi:10.1002/2013JD021108, 2014.

Zhang, Q., Geng, G. N., Wang, S. W., Richter, A. and He, K. Bin: Satellite remote sensing of changes in NO x emissions over China during 1996-2010, Chinese Sci. Bull., 57(22), 2857–2864, doi:10.1007/s11434-012-5015-4, 2012a.

Zhang, R., Wang, G., Guo, S., Zamora, M. L., Ying, Q., Lin, Y., Wang, W., Hu, M. and Wang, Y.: Formation of Urban Fine Particulate Matter, Chem. Rev., 115(10), 3803–3855, doi:10.1021/acs.chemrev.5b00067, 2015.

Zhang, X., van Geffen, J., Liao, H., Zhang, P. and Lou, S.: Spatiotemporal variations of tropospheric SO 2 over China by SCIAMACHY observations during 2004-2009, Atmos. Environ., 60, 238–246, doi:10.1016/j.atmosenv.2012.06.009, 2012b.

Zhang, Y.-L. and Cao, F.: Fine particulate matter (PM 2.5) in China at a city level., Sci. Rep., 5, 14884, doi:10.1038/srep14884, 2015.

Zhang, Y. H., Hu, M., Zhong, L. J., Wiedensohler, a., Liu, S. C., Andreae, M. O., Wang, W. and Fan, S. J.: Regional Integrated Experiments on Air Quality over Pearl River Delta 2004 (PRIDE-PRD2004): Overview, Atmos. Environ., 42(25), 6157–6173, doi:10.1016/j.atmosenv.2008.03.025, 2008.

Zhong, L., Louie, P. K. K., Zheng, J., Yuan, Z., Yue, D., Ho, J. W. K. and Lau, A. K. H.: Science–policy interplay: Air quality management in the Pearl River Delta region and Hong Kong, Atmos. Environ., 76, 3–10, doi:10.1016/j.atmosenv.2013.03.012, 2013.

Zotter, P., El-haddad, I., Zhang, Y., Hayes, P. L., Zhang, X., Lin, Y., Wacker, L., Schnelle-kreis, J., Abbaszade, G., Zimmermann, R., Surratt, J. D., Weber, R., Jimenez, J. L., Szidat, S., Baltensperger, U. and Prévôt, A. S. H.: Journal of Geophysical Research : Atmospheres, , 1–18, doi:10.1002/2013JD021114.Received, 2014.

Zou, Y., Deng, X. J., Zhu, D., Gong, D. C., Wang, H., Li, F., Tan, H. B., Deng, T., Mai, B. R., Liu, X. T. and Wang, B. G.: Characteristics of 1 year of observational data of VOCs, NO_x and O_3 at a suburban site in Guangzhou, China, Atmos. Chem. Phys., 15(12), 6625–6636, doi:10.5194/acp-15-6625-2015, 2015.

Atmos. Chem. Phys. Discuss., doi:10.5194/acp-2017-116, 2017
Manuscript under review for journal Atmos. Chem. Phys.
Discussion started: 15 March 2017

Table 1 Elemental ratios of organic PM_1 in PRD

Site/ characteristics	Month	Aiken-Ambient (A-A) method			Improved-Ambient (I-A) method			Reference
		O:C	**H:C**	**OM:OC**	**O:C**	**H:C**	**OM:OC**	
Panyu/suburban	November	0.42	1.49	1.71	0.53	1.63	1.87	This study
	December	0.41	1.5	1.70	0.53	1.65	1.87	
Kaiping/rural	November	0.47	1.48	1.77	0.60*	1.64*	1.94*	Huang et al., 2011
Shenzhen/Urban	November	0.3	1.63	1.57	0.38*	1.81*	1.66*	He et al., 2011
Heshan/Rural	November	0.4	1.49	1.72	0.51*	1.65*	1.83*	Gong et al., 2012
HKUST/Suburban	February	0.42	1.39	1.71	0.53*	1.54*	1.86*	Li et al., 2015
	December	0.43	1.4	1.71	0.55*	1.55*	1.87*	
Mong Kok/Urban	March-mid May	0.25	1.68	1.49	0.32	1.84	1.59	Lee et al., 2015

* Improved-Ambient elemental ratios were estimated from the A-A method with the empirical constants from M. R. Canagaratna et al. 2015

Atmos. Chem. Phys. Discuss., doi:10.5194/acp-2017-116, 2017
Manuscript under review for journal Atmos. Chem. Phys.
Discussion started: 15 March 2017

Table 2 SOA-Ox average ratio comparison

Site	Month	Season	SOA-Ox average ratio	Reference
Panyu, Guangzhou	November	Late autumn	0.23 μg /(sm^3 ppb) *	This study
	December	Winter	0.25 μg /(sm^3 ppb) *	
Pasadena, CA	May-June (morning)	Late spring-summer	0.183 μg /(sm^3 ppb) *	Hayes et al., 2013
	May-June (afternoon)	Late spring-summer	0.163 μg /(sm^3 ppb) *	
Riverside, CA	July-August	summer	0.142 μg /(sm^3 ppb) *	Docherty et al., 2011
Mexico City	March	spring	0.156 μg /(sm^3 ppb) *	Aiken et al., 2009
New York City	July	summer	0.12 μg /(sm^3 ppb)	Sun et al., 2011

*The volume unit "sm" stands for volume under standard-temperature-pressure conditions

Atmos. Chem. Phys. Discuss., doi:10.5194/acp-2017-116, 2017
Manuscript under review for journal Atmos. Chem. Phys.
Discussion started: 15 March 2017

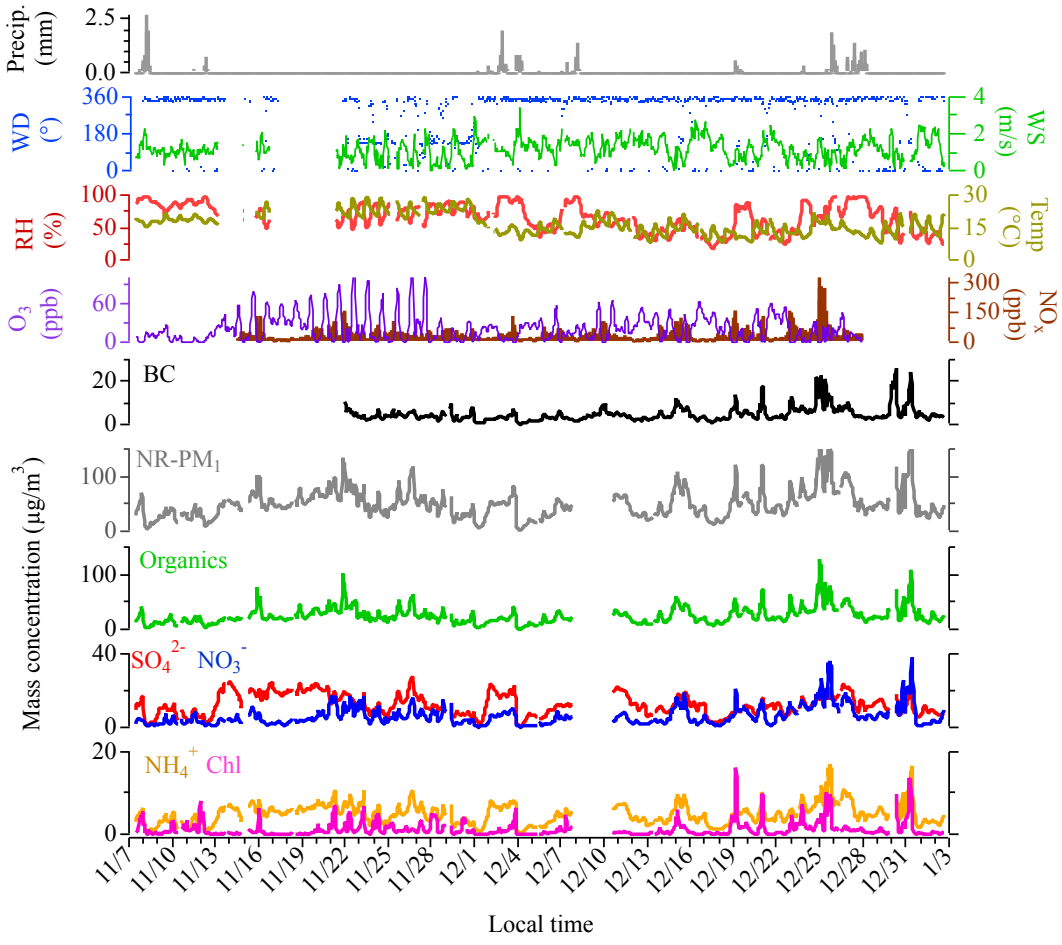

Figure 1 Time series of NR-PM$_1$ species (sulfate, nitrate, ammonium, chloride, and organics), BC, and meteorological factors (precipitation, relative humidity, temperature, wind direction and wind speed) for the campaign. Hourly averages are shown.

Atmos. Chem. Phys. Discuss., doi:10.5194/acp-2017-116, 2017
Manuscript under review for journal Atmos. Chem. Phys.
Discussion started: 15 March 2017

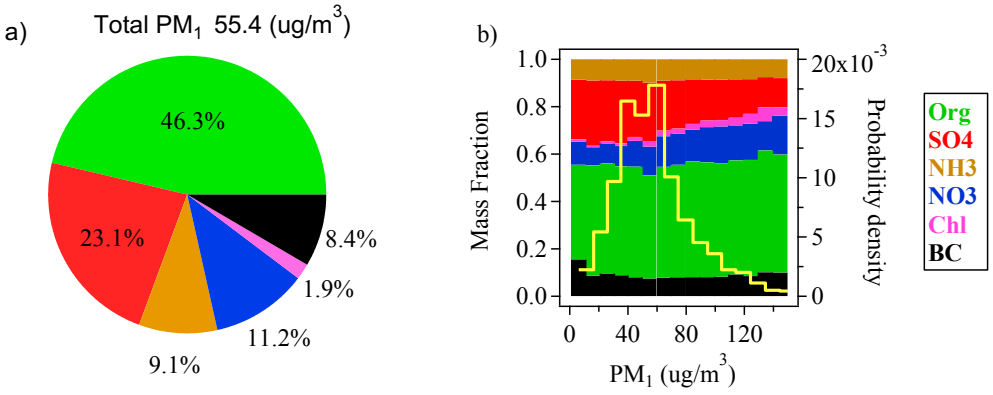

Figure 2a) Average mass fraction of PM_1 (with BC inclusive) during the whole campaign; b) Mass fraction variation of PM_1 species as well as the probability density of PM_1 as a function of total PM_1 mass loading. The probability density distribution describes the relative likelihood for the PM_1 mass loading in a certain range of concentrations.

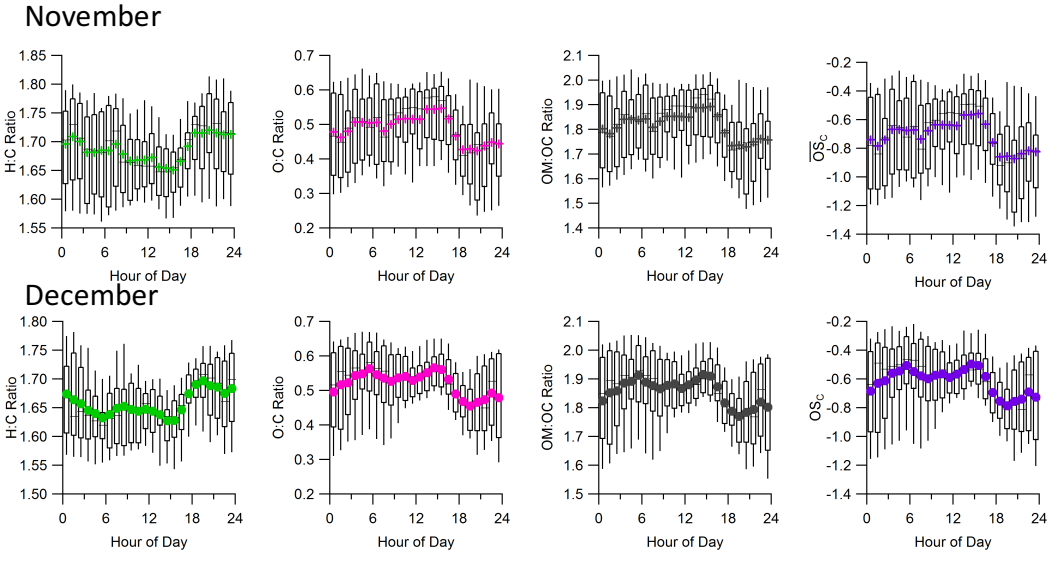

Figure 3 Diurnal variation of H:C and O:C OM:OC ratio and carbon oxidation state ($\overline{OS_c} \approx 2\times$O:C-H:C) during Nov. and Dec. (25th and 75th percentile boxes, 5th and 95th percentile whiskers, median as line in box, and mean as solid colored line).

Atmos. Chem. Phys. Discuss., doi:10.5194/acp-2017-116, 2017
Manuscript under review for journal Atmos. Chem. Phys.
Discussion started: 15 March 2017

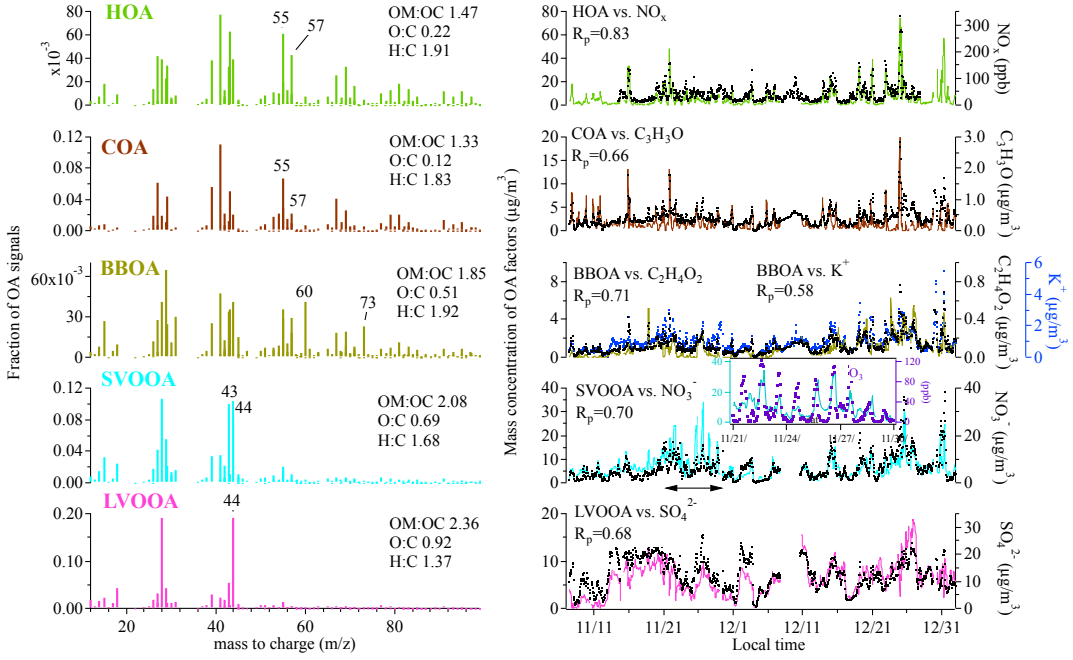

Figure. 4. The mass spectra of all OA factors and the time series of their mass concentrations together with external tracers.

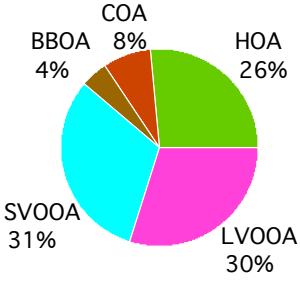

Figure 5. Campaign average mass fraction of each factor.

Atmos. Chem. Phys. Discuss., doi:10.5194/acp-2017-116, 2017
Manuscript under review for journal Atmos. Chem. Phys.
Discussion started: 15 March 2017

Atmospheric Chemistry and Physics
Discussions
Open Access

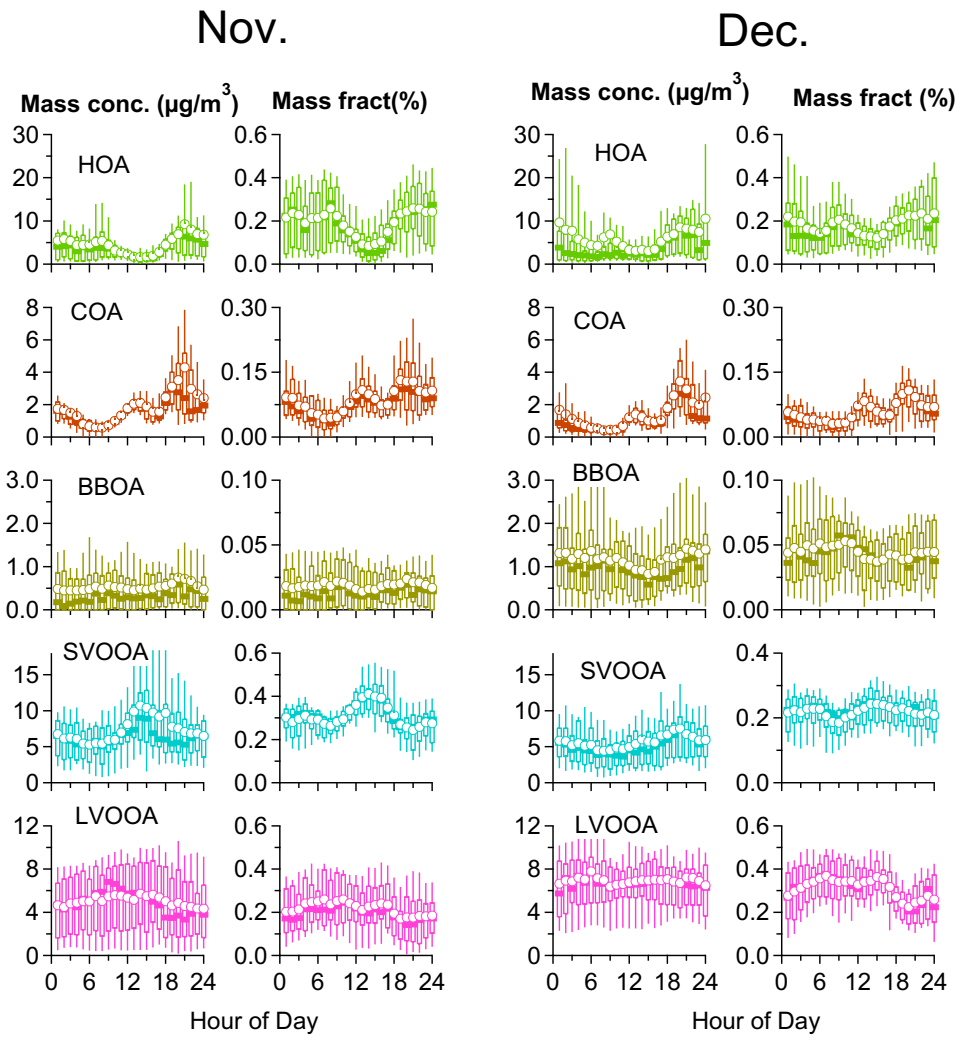

Figure 6 Diurnal variations of ME-2 resolved OA factors. Mass concentration of each OA factor (left). Mass fraction of each OA factor (right). 25th and 75th percentile boxes, 5th and 95th percentile whiskers, median as line in box, and mean as solid colored line.

Atmos. Chem. Phys. Discuss., doi:10.5194/acp-2017-116, 2017
Manuscript under review for journal Atmos. Chem. Phys.
Discussion started: 15 March 2017

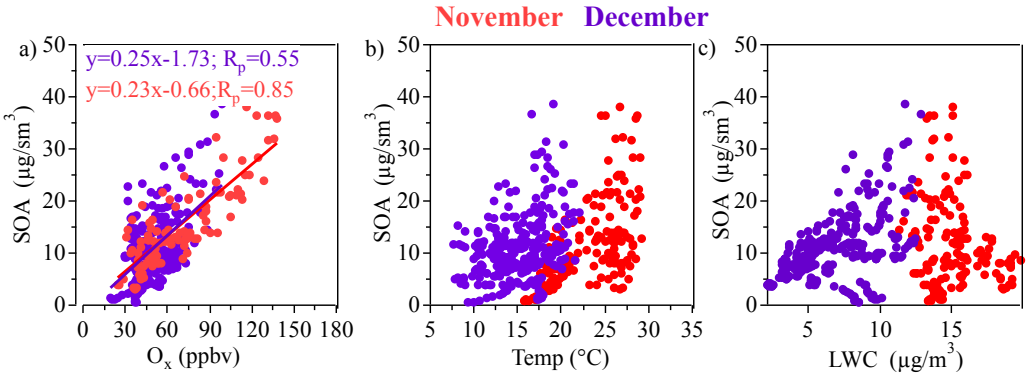

Figure 7 (a)SOA against Ox; (b)SOA against temperature; (c) SOA against LWC during daytime.. The concentration of SOA has been converted to standard-temperature-pressure conditions in order to compare the slope of SOA/Ox with literature values.

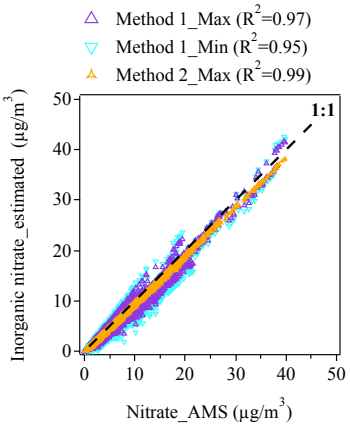

Figure 8 Scatter plot of estimated inorganic nitrate versa nitrate from HR-ToF-AMS measurement.

Atmos. Chem. Phys. Discuss., doi:10.5194/acp-2017-116, 2017
Manuscript under review for journal Atmos. Chem. Phys.
Discussion started: 15 March 2017

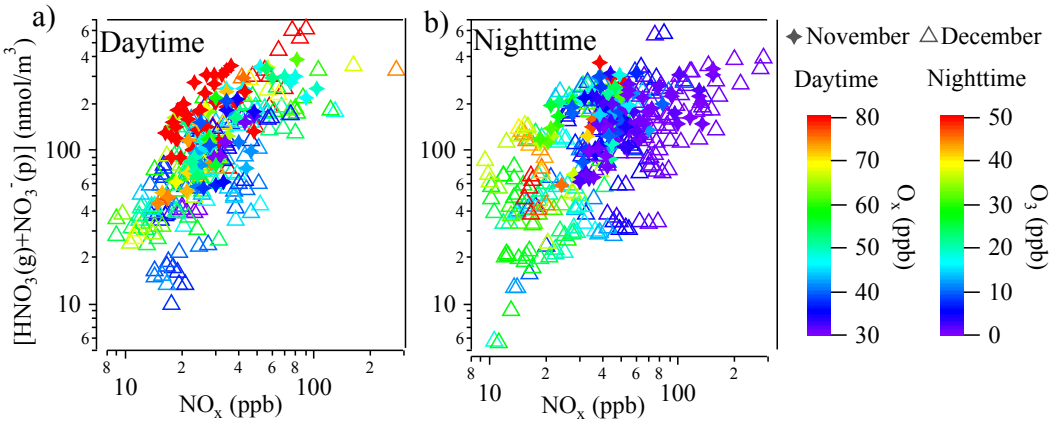

Figure 9 Correlations between total nitrate（$HNO_3(g)$+ NO3(p)) and NO_x ($NO+NO_2$). Triangles and circles represent data for November and December respectively. Data are color-coded by O_x during daytime and O_3 during nighttime.

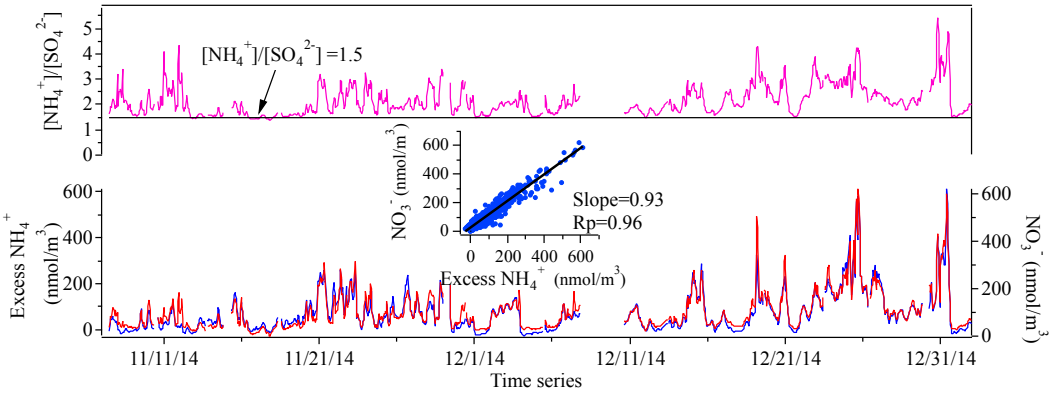

Figure 10 Time series of nitrate, excess NH4 and NH4-to-SO4 molar ratio.

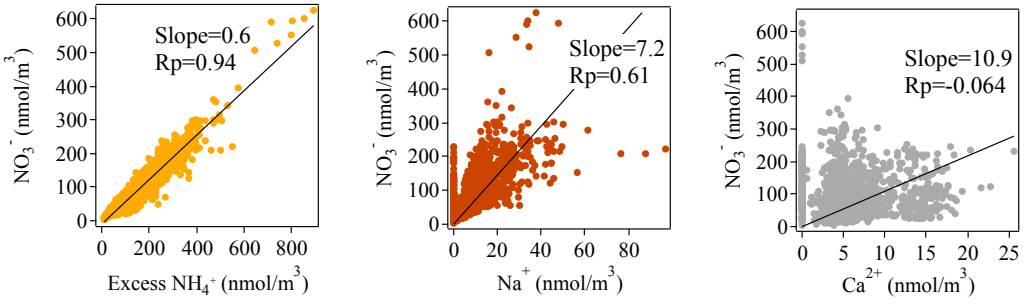

Figure 11 Scatter plots of NO_3^-molar concentration from MARGA ($PM_{2.5}$) against those of Excess NH_4^+, Na^+ and Ca^{2+}.

Atmos. Chem. Phys. Discuss., doi:10.5194/acp-2017-116, 2017
Manuscript under review for journal Atmos. Chem. Phys.
Discussion started: 15 March 2017

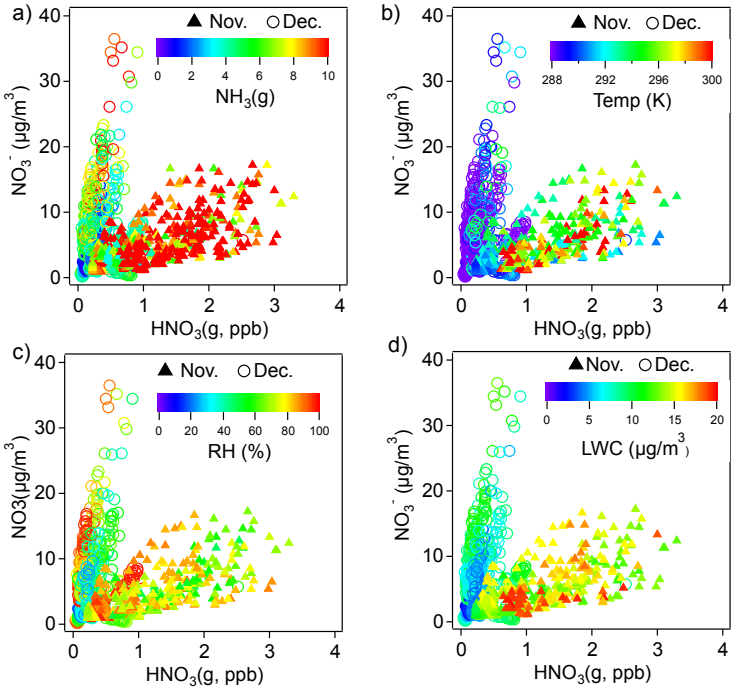

Figure 12. Distribution of nitrate species between $HNO_3(g)$ and $NO_3^-(p)$. Colored by (a)NH_3 concentration (b) temperature, (c) R (d) LWC.